Role of surfactant molecules in magnetic fluid: Comparison of Monte Carlo simulation and electron magnetic resonance

L. L. Castro, G. R. R. Gonçalves, K. Skeff Neto, and P. C. Morais
Instituto de Física, Universidade de Brasília, Caixa Postal 04455, CEP 70917-970, Brasília, DF, Brazil

A. F. Bakuzis
Instituto de Física, Universidade Federal de Goiás, CEP 74001-970, Goiânia, GO, Brazil

R. Miotto
Centro de Ciências Naturais e Humanas, Universidade Federal do ABC, Rua Santa Adélia, 166, CEP 09210-170, Santo André, SP, Brazil

(Received 13 November 2007; revised manuscript received 22 November 2008; published 31 December 2008)

We investigate a magnetic fluid composed of magnetite nanoparticles surfacted with dodecanoic acid molecules and stably dispersed in a hydrocarbon solvent. A comparison between Monte Carlo simulation and different experimental techniques allows us to validate our methodology and investigate the behavior of the surfactant molecules. Our analysis, based on the Langmuir model, suggests that the surfactant grafting number on isolate nanoparticles increases with the nanoparticle concentration, while the grafting on agglomerated nanoparticles presents a more complicated behavior. Our results suggests that, if properly coated and at a certain concentration range, colloids can become stable even in the presence of agglomerates. The role of the Hamaker constant, which controls the van der Waals interaction intensity, was also investigated. We have found that the ratio between grafting and Hamaker constant governs the level of nanoparticle agglomeration.

DOI: 10.1103/PhysRevE.78.061507 PACS number(s): 83.80.Qr, 47.65.Cb, 68.43.Mn, 47.57.−s

I. INTRODUCTION

Magnetic fluids (ferrofluids) are colloidal dispersions of magnetic nanoparticles, whose biomedical applications have been the subject of a great variety of studies [1–3]. When directly exposed to oxygen, magnetite nanoparticles may undergo degradation, resulting in the alteration of their magnetic properties. Additionally, like any other colloidal suspension, magnetic nanoparticles may form large agglomerates that eventually flocculate. In order to avoid both degradation and excessive aggregation, which could destroy the stability of the magnetic fluid, the nanoparticles are usually coated by a neutral surfactant layer (surfacted magnetic fluids) or an ionic layer (ionic magnetic fluids). In surfactant-stabilized ferrofluids, the stability of the suspension is provided by the steric hindrance of the surfactant molecules that counteracts the dipolar and van der Waals attraction among the magnetic nanoparticles, producing a dispersion of the particles with randomly oriented magnetic moments [4]. Amphiphilic molecules, such as oleic acid and aerosol sodium di-2 ethylhexyl-sulfosuccinate, are examples of surfactant agents that produce steric repulsions. Ionic surfactants such as tetramethylammonium hydroxide can be used as a surfactant that produces electrostatic repulsion in an aqueous medium.

Besides their importance in colloidal stability, surfactant effects play a key issue in the further functionalization of the nanoparticle, as the bioactivity is often related to a protein bounded to the nanoparticle's coating layer [3]. In this sense, the interaction of the nanoparticle's coating with the protein or antigen that will be used in order to achieve its bioactivity is crucial in its design. In order to allow a better understanding of the further functionalization of the stabilized coated nanoparticle, the surfacting process must be understood. Indeed, recently our group has dedicated great efforts in the experimental understanding of the grafting process of the nanoparticle first molecular layer [5–7], with a view to contribute to the effectiveness of binding specific biomolecules in the final stages of the synthesis of biocompatible magnetic fluids. However, the development of a given protocol with all production steps (from the synthesis to the functionalization of drugs) of a nanoparticle can be very expensive and time-consuming. Computer simulations, on the other hand, can be easily repeated with different parameters and can thus be an useful tool in testing novel designs and potential functionalization surfactants. As the size of usual nanoparticles is around 10 nm, quantum chemistry calculations are not within the capability of available computers. An interesting alternative for accessing the properties of such systems are Monte Carlo simulations.

Monte Carlo simulations of magnetic fluids are not new [8]. Indeed, in 1982, bidimensional simulations of magnetic fluids were already performed [9], using a simple model, which does not take into account van der Waals interactions and which has been used until recent years [10]. The evolution of this kind of simulation included extensions to tridimensional systems [11–13], *cluster moving algorithms* [12,14], and the addition of new potential terms, such as the van der Waals [15] and the Lennard-Jones potentials [16]. However, in most cases, including very recent publications [17–19], usually no direct comparison between Monte Carlo simulations and experimental data is done. In fact, in the majority of these works only dipolar interactions are considered [20]. One exception is the interesting paper by Kruse *et al.* [15] where small-angle x-ray scattering (SAXS) data [21] were compared with Monte Carlo simulations. In this paper van der Waals and dipole-dipole interactions and a simplified version of the steric repulsion were taken into account.

Previous Monte Carlo simulations of magnetic fluids suggested that nanoparticles tend to agglomerate

[9,10,12,14–16,22]. In some of these simulations, the formation of long chains is observed when high concentrations of large nanoparticles are considered [9,10,22] and a strong external magnetic field is applied [9,22]. The formation of long magnetic nanoparticles chains was first suggested by de Gennes and Pincus [23]. However, long chains were never clearly identified in experimental measurements. Indeed, experimental investigations on magnetic fluids detected only the formation of small agglomerates [21,24–26], typically formed by two to four nanoparticles. This was further confirmed by a size-bidisperse model [27], heterophase fluctuations [28], and chain formation model with modified mean-field-theory [29] based simulations.

Our aim in this work is to present a more complete Monte Carlo simulation of real magnetic fluids in order to allow a better prediction of their properties, helping to concentrate the experimental efforts in the most promising systems. For doing so, our model includes magnetic, van der Waals, and Zeeman magnetic interactions. In addition, as in our simulations we are also interested in aspects closely related to the interactions between surfactant layers, the *steric* repulsion between adsorbed molecules was also included following the model of Mackor [30,31]. We should stress that this contribution was only correctly taken into account by Chantrell *et al.* [9], who performed two-dimensional Monte Carlo simulations of monodisperse magnetic fluids. However, the authors did not include the van der Waals interaction term. In the present work we consider three-dimensional polydisperse magnetic fluids including all the interaction terms. We will show that, together with van der Waals interaction, the steric contribution plays a key role in the microstructure of chain formation of colloids. The present paper is organized as follow: in Sec. II, we describe the magnetic resonance experiment, our model for surfacted magnetic fluids, and a description of the parameters used in our simulations; in Sec. III, our results are compared to experimental data obtained by our group in order to validate the methodology, from which we estimated the value and the concentration dependence of the density of surfactant molecules of isolated nanoparticles and agglomerates; in addition, the influence of the Hamaker constant (A) is considered. A systematic comparison of all calculated properties is done considering different values of A. Our simulations suggest that the relation between grafting and the Hamaker constant governs agglomeration when other parameters are kept fixed, at least when the values of A are in the range considered in the present work.

II. METHOD

A. Experiment

The electron magnetic resonance (EMR) technique has been widely used to investigate the magnetic properties of nanorods [32], biomimetic nanoparticles [33], nanocomposites [34,35], and magnetic fluids [36–38]. The latter are the focus of the present article. EMR spectra were taken at room temperature using a commercial Bruker ESP300 cw spectrometer tuned around 9.4 GHz. From EMR analysis it was possible to extract information about the surface-surface particle's distance of nanoparticles forming small agglomerates [38,39] or the fraction of monomers (isolated nanoparticles) and agglomerates in the magnetic fluid as a function of the nanoparticle's concentration. The information obtained from the EMR analysis would be then compared with our Monte Carlo simulations. Note that a previous EMR analysis has been published before in Ref. [39], but the present results considered not only a wider particle concentration range, but also investigated the fraction of agglomerates as discussed later in the text. The magnetite nanoparticles were obtained by chemical precipitation of a mixture of iron (II) and iron (III) ions in an alkaline aqueous medium. Peptization and stabilization of the magnetic precipitate were performed by surface coating the magnetite nanoparticles with dodecanoic acid and stably dispersing them in hydrocarbon following a well-established method from the literature [40].

B. Monte Carlo simulation

Monte Carlo is a label used to designate stochastic methods for solving mathematical problems. Systems that follow the Boltzmann energy distribution can be simulated by means of the Metropolis algorithm [41], which starts from a random configuration of the system and performs successive small variations in all its coordinates. The procedure is as follows: (a) For each variation, the change ΔE in energy is calculated. (b) If the value of the new potential energy is lower than the previous one, the new configuration is accepted. (c) If it is higher, a random number between 0 and 1 is generated and compared with the factor $e^{-\Delta E/k_BT}$. The new configuration is accepted only if the random number is lower than this factor. Steps (a)–(c) are then repeated, and after a period of energy stabilization, the average value of the properties of interest are computed over all accepted configurations. This procedure guarantees that the accepted configurations follow the Boltzmann energy distribution $ke^{-\Delta E/k_BT}$ (where k is a normalization constant), and therefore the calculated average values represent the most probable values for the respective properties. For the magnetic fluid system simulated in this work, a configuration is determined by the positions of the nanoparticles and the orientations of its magnetic dipole moments. Therefore, in each iteration of the Metropolis algorithm, both the positions and the orientations of the magnetic dipole moments of all considered nanoparticles experience a random change.

In our model, each nanoparticle is considered as a perfect sphere [8], consisting of a rigid magnetic core and a softlike coating layer that reacts to the presence of other nanoparticles in the system by means of the following interactions: (a) *magnetic*, with punctual dipoles centered in each sphere; (b) *van der Waals*, which consists of attraction between instantaneous electric dipoles resulting of fluctuations and other electric dipoles induced by the first ones; (c) *steric repulsion*, which appears when the surfactant layers of two nanoparticles are placed in contact. In addition, the (d) *Zeeman magnetic interaction* of each magnetic dipole moment with an external applied magnetic field is also considered.

In order to perform the Metropolis algorithm, it is necessary to explicitly define expressions for these potential energies associated with these interactions. For two nanoparticles with indices i and j, the potential energy associated with the magnetic dipole interaction can be written as

$$U_d(ij) = \frac{\mu}{4\pi}\left(\frac{\vec{m}_i \cdot \vec{m}_j}{r^3} - 3\frac{(\vec{m}_i \cdot \vec{r}_{ij})(\vec{m}_j \cdot \vec{r}_{ij})}{r^5}\right), \quad (1)$$

where μ is the magnetic permeability of the solvent, $\vec{m}_i$ and $\vec{m}_j$ are the magnetic dipole moment vectors of the particles i and j, respectively, and r is the modulus of $\vec{r}_{ij}$, which represents the position of i in relation to j. The energy associated with the van der Waals interaction is defined as [42]

$$U_v(ij) = -\frac{A}{12}\left[\frac{D_{ij}^2}{r^2} + \frac{D_{ij}^2}{r^2 - D_{ij}^2} + 2\ln\left(\frac{r^2 - D_{ij}^2}{r^2}\right)\right], \quad (2)$$

where A is the Hamaker constant and D_{ij} is the average diameter for nanoparticles i and j. The energy associated with the steric repulsion is given by [30,31]

$$U_s(ij) = \begin{cases} \frac{\pi\xi k_b T}{2} D_{ij}^2 \left[2 - \frac{l}{t} - \frac{l+2}{t}\ln\left(\frac{1+t}{1+\frac{l}{2}}\right)\right] & \text{if } (s/2\delta) \leqslant 1, \\ 0 & \text{if } (s/2\delta) > 1, \end{cases} \quad (3)$$

where ξ is the so-called "grafting"—i.e., the surface density of adsorbed molecules in the nanoparticles—s is the surface-surface distance, δ is the width of the surfactant layer, $l = 2s/D_{ij}$, and $t = 2\delta/D_{ij}$. For a pair of nanoparticles with 10 nm in diameter, at a temperature of 300 K, considering the head-to-tail configuration, this potential falls from $30k_BT$ to 0 in the range $s = 0 - 2\delta$. The Zeeman interaction between each magnetic dipole moment and the magnetic field is represented by

$$U_B(i) = -\vec{m}_i \cdot \vec{B}. \quad (4)$$

In order to avoid the transient region, convergence tests are made after a minimum of 300 000 iterations in a given simulation are disregarded. Average values are calculated only after the total energy does not decrease by more than 10% for 5000 consecutive accepted configurations. After the convergence criteria is reached, the averages are computed considering at least 100 000 sampling iterations and a new convergence test is performed: if the total energy of the accepted configurations does not decrease by more than 1%, the simulation stops. We have followed a large number of simulations where both convergence criteria were reached when 300 000 thermalization iterations and 100 000 sampling iterations were performed.

C. Description of the nanoparticles

In this work, we focus on the properties of nanoparticles with magnetite (Fe_3O_4) cores and with dodecanoic acid ($C_{12}H_{24}O_2$) as surfactant agent, dispersed in a hydrocarbon solvent (C_nH_m). This system was characterized by our group using several techniques [39,43]. From previous EMR experimental measurements, it was possible to extract the fraction of monomers [43] and the surface-surface distance of nanoparticles forming agglomerates [39]. Different nanoparticles concentrations were experimentally obtained through evaporation or dilution of the solvent, while different surfactant coverages (grafting) can be achieved changing the surfactant agent concentration during the nanoparticle's synthesis. Therefore, in our simulations a systematic investigation of all these quantities is performed in order to allow a direct comparison between theory and experiment. Special attention is dedicated to the grafting, as any further functionalization and hence the biological activity will be directly influenced by these quantity. The grafting (ξ) is defined as the surface density of molecules adsorbed on the nanoparticle. In order to perform a systematic study of the grafting influence in the system's properties, we have considered a large range of grafting values: from 1×10^{16} molecules/m^2 to 1×10^{19} molecules/m^2. The value of the Hamaker constant (A) was initially fixed in 4×10^{-20} J. This is slightly below the 5×10^{-20} J assumed by Kruse *et al.* [15] after observing nonconvergence of the potential energy for higher values of this constant. From a simple geometric method, based on molecular orbitals, the thickness of the dodecanoic acid surfactant layer was calculated to be 1.2 nm. This is consistent with the estimated value of 0.8 nm by Bonini and co-workers [4] via small-angle scattering of polarized neutrons and so will be kept fixed throughout this work. The considered external magnetic field was in the range 0 to 0.3 T, as this last value was found [39,43] to be of the order of the magnetic resonance field.

A dodecanoic acid molecule is composed of a (═O—OH) polar head and an hydrocarbon apolar tail. Raman spectroscopy results [6,7] show that dodecanoic acid molecules adsorb on magnetite-based nanoparticle surfaces when dispersed in hydrocarbon, but the effective hydroxyl grafting coefficient for this system is much smaller than the observed for other surfactant molecules [7], suggesting that they could desorb, depending on the circumstances. In an isolated nanoparticle, the more stable configuration is characterized by the attachment of the polar heads of the dodecanoic acid molecules to the surfaces of the nanoparticles, while the apolar tails remain in contact with the hydrocarbon solvent. When agglomerates are formed, the situation is more complex, as the surfactant layers are superimposed. In this situation, the attachment of the molecules on the surface might be no longer favorable resulting in their desorption.

The particle size polydispersity profile of the sample was obtained from transmission electron microscopy (TEM) micrographs using a Jeol 100CXII system. From the electron microscopy data, we obtained a modal diameter of 8.9 nm and a diameter dispersity of 0.34, using a log-normal distribution function to fit the TEM data [39]. As polydispersity has an influence on the properties of the ferrofluid, in particular also on the equilibrium magnetization [8], in our simulations the nanoparticle's diameters also follow a log-normal distribution [39], whose probability density is

$$f_{log\ normal}(D) = \frac{\exp(-2\sigma^2)}{D_{f_{max}}\sigma\sqrt{2\pi}}\exp\left(-\frac{\ln^2(D/D_{f_{max}})}{2\sigma^2}\right), \quad (5)$$

where D is the diameter variable, σ is dispersion parameter (the higher σ is, the more dispersed the diameters are), and $D_{f_{max}}$ is the modal diameter—i.e., the most probable diam-

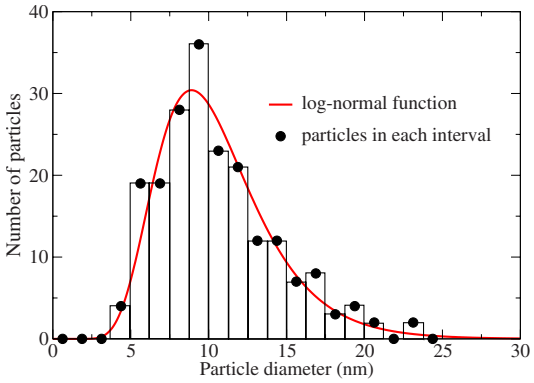

FIG. 1. (Color online) Histogram built using an ensemble of 200 nanoparticle's diameters obtained following the procedure described on Ref. [44]. The log-normal function, represented by a solid red (gray) line, is multiplied by a scale factor which provided the best adjustment to the points. The number of histogram bars and their width are arbitrary and merely illustrative, as long as, actually, a different set of 200 different diameters was generated for each simulation.

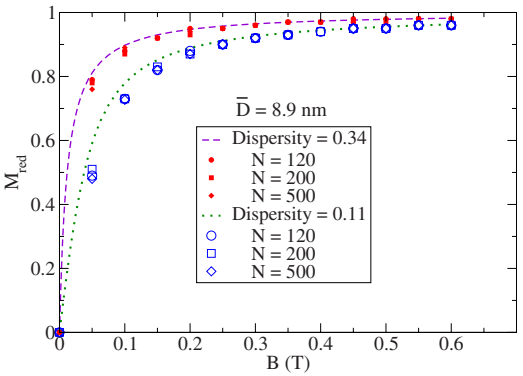

FIG. 2. (Color online) Reduced magnetization curves for the simulated magnetic fluid, considering a concentration (in volume fraction) $\phi=0.0029$. The dashed line is the generalized Langevin curve for $\sigma=0.34$, and the dotted one is for $\sigma=0.11$. The solid and open symbols are the corresponding simulations for different number of particles: circles for $N=120$, squares for $N=200$, and diamonds for $N=500$.

eter. In the simulations, this distribution was obtained via a Metropolis-like algorithm as previously reported [44]. Figure 1 shows a histogram built using 200 diameters generated by this algorithm and a comparison with a log-normal curve with $D_{f_{max}}=8.9$ nm and $\sigma=0.34$. Good agreement between our calculated diameter distribution and the log-normal function is clearly seen here.

III. RESULTS AND DISCUSSION

The main aspect of magnetic fluids that makes them interesting for applications is their response to external magnetic fields. In this sense, magnetization curves (magnetization versus magnetic field) are excellent candidates for the first test of our simulation procedure. As the average properties might be influenced by the number of nanoparticles considered in each simulation, we have also used the magnetization curves to establish this number by plotting the curves for different numbers of particles. The magnetization (M) of the system is calculated by summing up the magnetic-dipole moment components in the direction of the external magnetic field and dividing it by the sample volume. A way of making magnetization calculations independent of concentration is calculating the reduced magnetization (M_{red})—i.e., the magnetization of the system divided by the saturation magnetization—corresponding to the case where all the magnetic-dipole moment vectors are completely aligned with the external magnetic field and can be calculated as the volume fraction (ϕ, volume occupied by nanoparticles divided by the total sample volume) times the bulk magnetization of the nanoparticles, in this case the magnetization of the magnetite, so $M_{sat}=\phi M_{Fe_3O_4}$. In Fig. 2 we present magnetization curves for samples with two different diameter dispersions ($\sigma=0.11$ and $\sigma=0.34$), modal diameter $D_{f_{max}}=8.9$ nm, and volume fraction $\phi=0.0029$. Our simulations indicate that $M_{red}(=M/M_{sat})$ does not change considerably for the three numbers of particles used: namely, $N=120$, 200, and 500. In order to save computational resources, we have chosen $N=200$ for all the subsequent simulations, following other studies where similar values of N where chosen [10,45]. For smaller magnetic fields, the results of our simulations are slightly below the calculated polydisperse Langevin curves (presented as dashed and dotted lines), which describe the limit in which the particles do not interact with each other. A similar underestimation of the magnetization was observed by Kristóf and Szalai [16]. This behavior is a result of the discretization of the log-normal curve, as recently suggested by Ivanov and co-workers [46]. They showed that this deviation can be reduced by improving the discretization. In the present case, due to the stochastic aspect of our discretization, this could be done simply by increasing the number of nanoparticles. However, considering that our main goal is the analysis of the system in the high-magnetic-field regime (0.3 T), where such deviations are very small, we have kept the number of nanoparticles fixed as 200 throughout our simulations in order to make them feasible. Therefore it is fair to say that our model yields the expected magnetization behavior in the high-magnetic-field regime. Finally, the fluctuation observed in all curves involving quantities of interest are small enough to allow us to focus on systematic variations.

Having obtained good agreement between the simulations and the theoretical results, the next step of our study was to compare the results of the simulations with experimental data. These data include the fraction of monomers F_{mon}—i.e., the fraction of particles that remain isolated—and the mean surface-surface distance $D_{surf\text{-}surf}$ in pairs of "bonded" nanoparticles, where bonded was defined as "with the surfactant layers in contact" ($0<s<2\delta$), and are discussed below.

Figure 3 shows the magnetic resonance spectrum for different nanoparticle concentrations of the magnetic fluid using an X band tuned around 9.4 GHz. Note that for the lower-concentration sample we observed another line at the low-field range due to the presence of paramagnetic impurities in the capillary used to hold the sample. Open circles represent the experimental data, whereas the thicker solid line is the

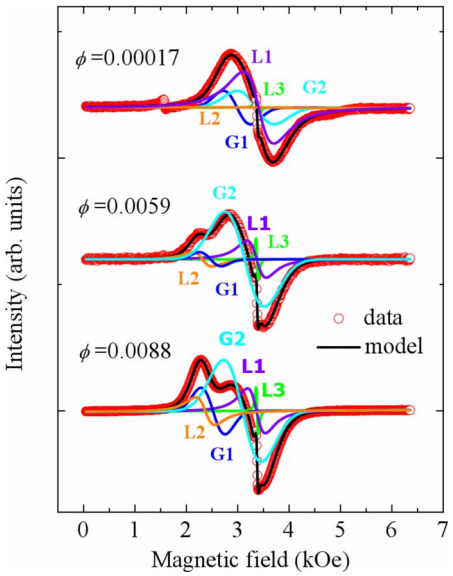

FIG. 3. (Color online) Magnetic resonance spectrum of the considered magnetic fluids with different volume fractions. The solid lines (G_1, G_2, L_1, L_2, and L_3) represent several contributions to the spectra obtained from the best fit of the experimental data.

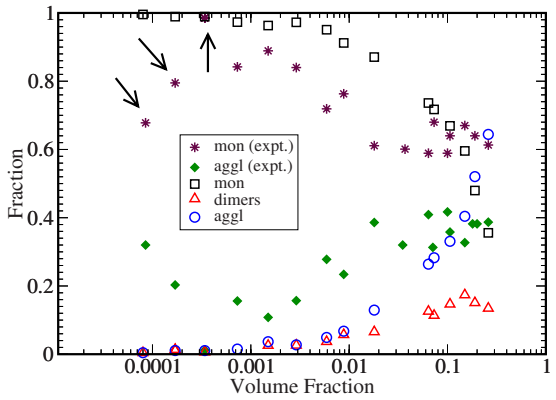

FIG. 4. (Color online) Comparison of simulated and experimental data for the fraction of monomers (mon), dimers, and agglomerates (aggl.) as a function of the particle volume fraction. Agglomerates include dimers in both cases, although dimers are also presented in an additional curve for the simulation data. The arrows indicate data points discussed in the text.

best fit using five components. The resonance components are Gaussian ($G1$ and $G2$) and Lorentzian ($L1$, $L2$, and $L3$) curves. The $L3$ component was attributed to the free-electron resonance as confirmed from the resonance field position, whereas the analysis of the others MR features showed contribution due to magnetic centers located in small agglomerates as will be discussed in the text. From our previous works [39,43] we were able to conclude that the contributions $L1$ and $G2$ most likely represent isolated particles (monomers), whereas the lines $L2$ and $G1$ are related to strongly and intermediary coupled small agglomerates. As the area is proportional to the density of magnetic centers in the magnetic structure, from its analysis we have obtained information about the fraction of monomers or agglomerates in the magnetic fluid sample. Figure 4 presents the fraction of monomers (purple stars) and agglomerates (green diamonds) obtained from this analysis, as well as simulated data discussed below. The experimental results in Fig. 4 clearly suggests that in the low-concentration regime the magnetic fluid consists mostly of monomers, while when the concentration increases the formation of small agglomerates is more likely to occur. The low occurrence of agglomerates and the prevalence of dimers in typical ferrofluid concentrations agree with the observations of other authors [24–26].

Recently Chen and co-workers [47] have found that the surface density of adsorbed molecules (grafting) on typical magnetic fluids is of the order of 10^{18} molecules/m^2. Therefore, we have used this typical value in order to obtain the fraction of monomers (black squares), fraction of dimers (red triangles), and fraction of agglomerates (blue circle) presented on Fig. 4. Note that while for the simulation agglomerate stands for systems composed by more than three nanoparticles, in the experimental analysis it is not possible to distinguish between dimers, trimers, tetramers, etc. Although the simulated and experimental numerical values are not identical, the curve profiles clearly present a very similar behavior, exception made to the experimental values obtained below a particle volume fraction of 0.000 34. Experimentally, for the two lowest particle concentrations a decrease of the fraction of monomers when the particle concentration decreases is observed. The region where this behavior occurs is represented in Fig. 4 by arrows. This result might be explained if we consider that a magnetic fluid can become unstable also in the low-concentration regime. Such behavior might be understood as a consequence of a decrease of the surfactant grafting at lower nanoparticle concentrations, probably due to the lower probability of a surfactant molecule to adsorb on a nanoparticle's surface. We believe that the decrease on the surfactant grafting is associated with a rupture of the dynamic equilibrium of the adsorption and desorption process on a given nanoparticle, caused by a high dilution of the system. A similar effect was experimentally observed through the analysis of the magnetic birefringence of magnetic fluids by Elói *et al.* [49]. It is also interesting to note that while the fraction of monomers continuously decrease with increasing concentration, the fraction of agglomerates are mainly due to dimers until a critical concentration range (around 1%). Above this limit, other types of agglomerates start to play a key role. It is well known that the origin of magnetic birefringence in magnetic fluids can be attributed to small agglomerates at this concentration range [24,25,50–52]. Our simulations agrees with this picture, and it is clear from Fig. 4 that there is a concentration range where most of the agglomerates consist of dimers.

In the next step of our study we compare the simulated and experimentally estimated values of the surface-surface particle distance ($D_{surf\text{-}surf}$). In order to allow a better understanding of how $D_{surf\text{-}surf}$ within an agglomerate is obtained, we briefly discuss the electron magnetic resonance field analysis. The resonance field (H_r) condition of interacting spherical nanoparticles is given by [38,39]

TABLE I. Comparison of the simulated (Theory) and experimentally estimated (Expt.) values of the surface-surface particle distance ($D_{surf\text{-}surf}$). All values are in nanometers (nm).

Volume fraction	Theory	Expt.
0.00034	2.29	4.6–6.3
0.0059	2.28	1.5–3.9
0.0088	2.28	1.6–4.1
0.064	2.29	2.1–5.1
0.073	2.28	2.1–5.3
0.1	2.29	1.2–4.6
0.15	2.28	1.7–4.1
0.19	2.28	1.9–4.3

$$H_r(\phi) = \frac{\omega}{\gamma\sqrt{1+\alpha}} - H_k - H_{int}(\phi), \tag{6}$$

where ω, γ, α, H_k, and H_{int} are the microwave frequency, gyromagnetic ratio, damping factor, magnetic anisotropy field, and interaction field, respectively. Note that increasing the particle concentration one expects a decrease of the resonance field due, primarily, to the dipolar field produced by neighboring nanoparticles. In fact, this behavior was already observed in our samples [39]. Indeed, remembering that the resonance field occurs at relatively high-field values, one can easily calculate the field due to a point dipole, $H_{int}^{dim} = \frac{2\mu}{r^3}$, where μ is the nanoparticle magnetic moment and r the center-to-center particle distance. Under this condition the dipole-dipole interaction always decreases the magnetic resonance field increasing the particle concentration. Since we had measured samples with different nanoparticles concentrations, we were able to find out by data extrapolation the resonance field at $\phi=0$. Therefore, it is straightforward to show that $H_r(\phi=0)-H_r(\phi)=H_{int}$. From this value one can easily calculate the particle-particle distance using

$$r = D\left(\frac{\pi M_s}{3[H_r(\phi=0) - H_r(\phi)]}\right)^{1/3}, \tag{7}$$

with D the mean particle diameter. In Table I, we present a comparison of the simulated and experimentally estimated values of the surface-surface particle distance between "bonded" nanoparticle pairs ($D_{surf\text{-}surf}$). We have considered M_s=471 G. While the theoretical value remains constant, the experimentally estimated values are distributed in a large range. A constant value for $D_{surf\text{-}surf}$ was not expected, since experimental data [53] clearly indicate a decrease of $D_{surf\text{-}surf}$ with increasing volume fraction. As all other comparisons between experimental and simulated data suggest that the grafting might play a decisively role in the magnetic fluid's properties, we decide to check out if this is indeed the case.

In order to identify the role of grafting on the surface-surface particle distance ($D_{surf\text{-}surf}$) and on the monomer distribution (F_{mon}), we have performed a systematic study where a large range of grafting (ξ) values are considered: from 1×10^{16} molecules/m^2 to 1×10^{19} molecules/m^2. Figures 5 and 6 present, respectively, $D_{surf\text{-}surf}$ and F_{mon} as a function of ξ for different concentrations. Each curve is fitted with the empirical expression $F(\xi)=X+W\tanh(Y\xi)$, where X, W, and Y are the adjusted parameters. In both graphs, the curves vary more significantly in the range $(1\times10^{17})-(1\times10^{18})$ molecules/m^2 and remains practically constant beyond these limits.

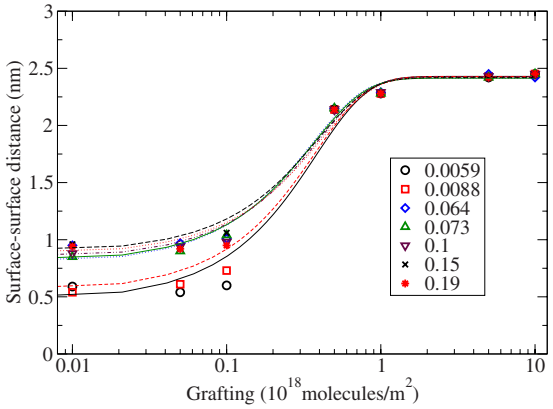

FIG. 5. (Color online) Surface-surface particle distance ($D_{surf\text{-}surf}$) as a function of the grafting (ξ). The expression $D_{surf\text{-}surf}(\xi)=X+W\tanh(Y\xi)$ was used to fit the curves. The legends show the concentrations, expressed as volume fractions, and the symbols or lines used for the correspondent simulation points.

As discussed previously, the number of nanoparticles (200) is kept fixed in all simulations and the box side is changed in order to obtain a given concentration. As the box side is considerably different when limit values (low and high concentrations) are compared, we have decided to check out the influence of the number of nanoparticles considered in the studied properties. For doing so, we have chosen a new constraint, not in the number of nanoparticles, but in the minimum side of the considered boxes: 150 nm. In this scheme, when the number of nanoparticles is increased, the box side is adjusted (with the 150 nm constraint) in order to obtain a given concentration. No noticeable variations on the considered properties are observed when the new set of

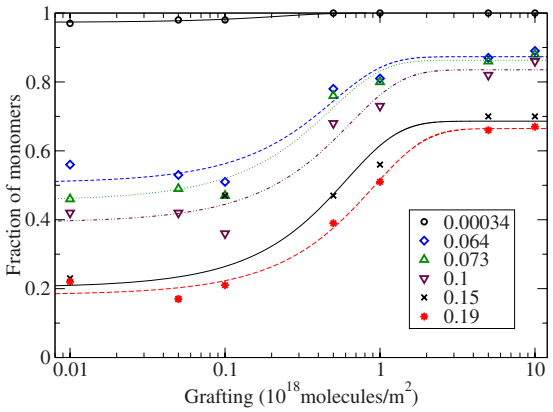

FIG. 6. (Color online) Fraction of monomers (F_{mon}) as a function of the grafting (ξ). The expression $F_{mon}(\xi)=X+W\tanh(Y\xi)$ was used to fit the curves. The legends show the concentrations, expressed as volume fractions, and the symbols or lines used for the correspondent simulation points.

TABLE II. Experimentally estimated range for $D_{surf\text{-}surf}$, calculated in various volume fractions, and the values of ξ for which the adjusted curves present the medium value of the range. This value was identified as the grafting of the agglomerated particles, ξ_{aggl}.

Volume fraction	$D^{expt}_{surf\text{-}surf}$ (nm)	ξ (10^{18} molecules/m^2)
0.0059	1.54	0.304
0.0088	1.62	0.317
0.064	2.12	0.535
0.073	2.11	0.537
0.1	1.20	0.121
0.15	1.72	0.309
0.19	1.86	0.401

TABLE III. Experimentally estimated range for F_{mon}, calculated in various volume fractions, and the values of ξ for which the adjusted curves present the medium value of the range. This value was identified as the grafting of the agglomerated particles, ξ_{mon}.

Volume fraction	F^{expt}_{mon}	ξ (10^{18} molecules/m^2)
0.00034	0.985	0.050
0.0059	0.719	
0.0088	0.763	
0.064	0.589	0.225
0.073	0.685	0.541
0.1	0.581	0.485
0.15	0.671	1.559
0.19	0.640	2.076
0.26	0.613	

simulations are compared with the previous ones. For the reduced magnetization, for example, increasing the number of particles from 200 to 500 and later to 800 did not change the calculated values by more than 1%. In a similar manner, increasing N (from 200 to 500 and later to 800) did not change the calculated fraction of monomers and the surface-surface particle distance ($D_{surf\text{-}surf}$) by more than 2% and 5%, respectively.

Using the adjusted curves, we made a comparison between experimental and simulation data in the following way: for each concentration, the value of ξ for which the experimental and simulated values of $F(\xi)$ are coincident is obtained. Surprisingly, the observed behavior is totally different depending on whether we used $F \equiv D_{surf\text{-}surf}$ or $F \equiv F_{mon}$—i.e., the adjusted curves for the fraction of monomers or those for the surface-surface distance. When F_{mon} is used, the grafting increases with increasing concentration, but for $D_{surf\text{-}surf}$, the behavior is more complex. This is shown in Tables II and III. Figure 7 shows the grafting as a function of the nanoparticle concentration extracted from these tables. This behavior can be understood if we consider that F_{mon} is mainly associated with the monomers, while $D_{surf\text{-}surf}$ is associated only with the agglomerated particles. In this sense, the crescent line can be associated with the grafting of the monomers (ξ_{mon}) and the other one with the grafting of the agglomerated nanoparticles (ξ_{aggl}).

Recently Chen *et al.* [47] used the Langmuir model to explain the grafting behavior of surfacted magnetic fluids. Note that the surfactant grafting is in fact a dynamic equilibrium situation between the surface desorption and adsorption processes of the molecular specie, which can be described by

$$C_{liquid} + N_{surface} \underset{k_\beta}{\overset{k_\alpha}{\rightleftarrows}} C{:}N_{adsorbed}. \tag{8}$$

This equation represents the dynamical adsorption process of a given coating molecule (C) on the nanoparticle surface (N) with a given set of adsorption (k_α) and desorption (k_β) rate constants. Following the so-called Langmuir kinetics model [54], the rate of adsorption (k_α) is proportional to the concentration of surfactant (which in our case is proportional to the coated nanoparticle volume fraction ϕ) and the number of available adsorption sites, while the desorption rate (k_β) is proportional to the number of adsorbed molecules. It is not difficult to show that the grafting number ξ according to the Langmuir model is given by [55]

$$\xi = \xi_{max} \frac{k\phi}{1 + k\phi}, \tag{9}$$

where $k = \frac{k_\alpha}{k_\beta}$. According to this model, the higher the particle volume fraction, the higher the grafting value. This is in qualitative agreement with our results for isolated nanoparticles. The solid line in Fig. 7 is the best fit according to the Langmuir model, where we have used the value of $\xi_{max} = 10.0 \times 10^{18}$ molecules/m^2 obtained from the literature [47], and only one parameter was used to fit the data. From the best fit we found $k_{monomers} = 1.06 \pm 0.17$, in qualitative agreement with the experimental data.

It is important to have in mind that this high value of ξ_{max} is a *high-package maximum*, corresponding to eight molecules adsorbed on a face of the magnetite spinel unit cell, considering a lattice parameter of 0.84 nm. Such a high grafting can only be achieved through a physisorption

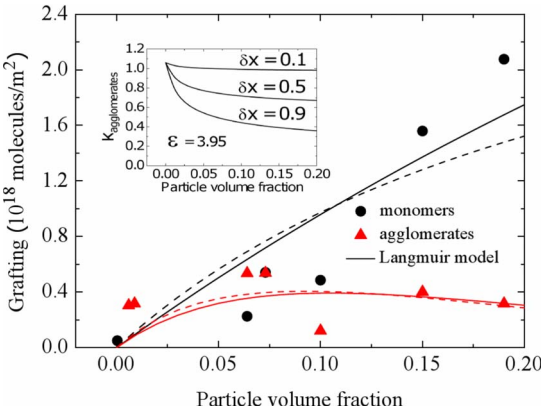

FIG. 7. (Color online) Grafting as a function of the particle volume fraction (ϕ). The solid (dashed) lines are obtained considering $\xi_{max} = 10.0 \times 10^{18}$ (3.5×10^{18}) molecules/m^2 In the inset, the adsorption rate (k_α) is presented as a function of the particle volume fraction considering an interaction parameter $\epsilon = 3.95$.

mechanism, when van der Waals bonds, which are not associated with specific sites, might play an important role. This view is consistent with the experimental analysis of Ref. [47], where the chemisorption mechanism was found to be more likely to be observed for low surfactant concentrations. As the surfactant concentration increases, the relevance of the physisorption is more significative. Another possibility which seems more likely is the chemisorption on one or more types of crystallographic surface sites. In that case, the local density of sites on a point on a nanoparticle surface depends on the local surface orientation relative to the preferential crystallographic direction. In principle, considering a surface deep of few angstroms, many sites are available for adsorption on each unit cell face. Klokkenburg *et al.* [48] measured graftings from 2 molecules/nm^2 to 3.5 molecules/nm^2, corresponding to 1.4–2.5 adsorbed molecules per unit cell. So we have fitted our data again considering a grafting of 3.5 molecules/nm^2. The dashed lines in Fig. 7 show the best fit in this case. We found that k changes from 1.06 ± 0.17 to 3.85 ± 1.05. The analysis of the statistical errors of the fitting parameters indicates that the fitting of the grafting of monomers is worst than obtained previously, and this is clearly seen by the inspection of Fig. 7. Although the result for the grafting of the monomers (dotted line) is not as good as our previous analysis (solid line), the model is obviously still valid.

It is clear that this model should be improved if the aim is to get a better quantitative agreement. Indeed, this quantitative error was already expected since the Langmuir model is based in several assumptions which the present system does not obey: the nanoparticle surface is certainly not flat, and the adsorption of the surfactant on a given site might also depends on the occupation of neighboring sites.

The particular behavior of the nanoparticles forming agglomerates can also be explained using the same model, but now noticing that $k_{agglomerates}$ should also depend on the particle volume fraction. This is because k depends on the number of available adsorption sites on the nanoparticle's surface. When two nanoparticles form agglomerates, the contact region represents a region where there are no available adsorption sites. One might also expect entanglement effects due to the interactions between the surfactant molecules [31]. The combination of those effects increases the number of surfactant molecules not adsorbed on a nanoparticle's surface, which again influences the grafting behavior. Nonadsorbed surfactant molecules might migrate to available surface sites on the nanoparticle's surface. In order to analyze the grafting behavior of nanoparticles forming agglomerates, we need first to estimate the mean size of agglomerates in our sample. This was done following the Zubarev-Iskakova model [56] on the zero-field condition:

$$\bar{Q} = \phi e^{\varepsilon} \left(\frac{1 - \dfrac{1 + 2\phi e^{\varepsilon} - \sqrt{1 + 4\phi e^{\varepsilon}}}{2\phi e^{\varepsilon}}}{\dfrac{1 + 2\phi e^{\varepsilon} - \sqrt{1 + 4\phi e^{\varepsilon}}}{2\phi e^{\varepsilon}}} \right), \tag{10}$$

with $\varepsilon = \frac{M_S^2 \pi^2 \langle D^3 \rangle}{18KT}$ the interaction parameter and $\langle D^3 \rangle = \int D^3 P(D) dD$. Considering the model; particle size as 8.9 nm and a size dispersion of 0.34, the interaction parameter was found to be 3.95. Using the fact that the number of available adsorption sites on agglomerates changes due to prohibited regions (i.e., regions where there are no available adsorption sites due to agglomeration), it is possible to estimate $k_{agglomerates}$ as

$$k_{agglomerates} = k_{monomers} \left(1 - \frac{\bar{Q} - 1}{\bar{Q}} \delta x \right), \tag{11}$$

where δx represents the percentage of prohibited adsorption sites due to agglomerate formation. The inset of Fig. 7 shows the calculated $k_{agglomerates}$ using the Zubarev-Iskakova model for the mean agglomerate size considering different δx values (for the zero-field condition and $k_{mon} = 1.06$). If δx is equal to zero (i.e., in the absence of entanglement effects or excluded adsorption sites), $k_{agglomerates}$ is equal to $k_{monomers}$, as expected. However, if δx is different from zero, $k_{agglomerates}$ decreases, increasing the particle volume fraction. $\bar{Q}$ is also a function of the magnetic field [56], which enhances the behavior discussed above. Indeed, comparison between experimental results and theoretical models from the literature shows only a qualitative agreement [52] between the theoretical models and the experimental mean agglomerate size. Therefore we used the following phenomenological expression:

$$k_{agglomerates} = k_{monomers} e^{-\alpha \phi}. \tag{12}$$

The solid (dashed) lines in Fig. 7 represent the best fit considering $\xi_{max} = 10.0 \times 10^{18}$ (3.5×10^{18}) molecules/m^2, maintaining the other parameters considered for the monomers and allowing α (α') to be fitted. With this set of parameters, we have found $\alpha = 9.5 \pm 2.2$ (10.8 ± 1.05). In both cases, isolated and agglomerates, the grafting concentration dependence has been satisfactory explained, although we used a very simple model in the analysis of our data. Indeed, our grafting values are also of the same order of those reported in the literature [47,48]. It is worthy pointing out that it was not possible to obtain a corresponding value of ξ for all volume fraction values on Tables II and III. This is because there were curves from the simulations whose obtained range of ξ did not include the available experimental values. This can be explained by realizing that our simulations make use of a very simplified model, which does not include hydrodynamic effects and depletion forces, as well as microscopic details of the nanoparticles. However, the qualitative behavior observed in those tables is coherent with what is expected from surfactant molecules.

It is well established that as concentration increases (during solvent evaporation process, for example), the level of agglomeration also increases. From our previous analysis, it is clear that the more agglomerated the particles are, the fewer adsorption sites are available to the surfactant molecules. In this sense, at higher concentrations, these molecules are more likely to desorb from an agglomerate system (especially due to the presence of prohibited adsorption sites) and migrate and adsorb on isolated adsorption sites. In other words, two distinct mechanisms are possible for desorbed molecules: they can attach to their original agglomerate, but away from the contact area, or they can attach to isolate nanoparticles. The comparison between our experimental re-

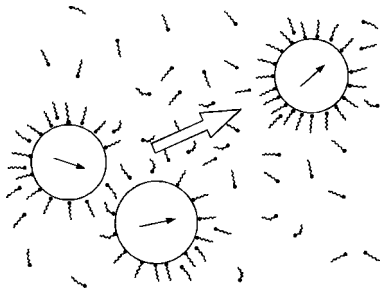

FIG. 8. When a pair of nanoparticles get close enough to put their surfactant layers in contact, the adsorbed molecules are taken out of their previous stability and tend to desorb from the surfaces of the nanoparticles. As the polar heads of the dissociated molecules are repelled by the apolar solvent, these molecules are more likely to adsorb on available adsorption sites of isolated particles or on the surface of the agglomerated particles. In the latter the adsorption will occur only on available adsorption sites far from the regions where the surfactant layers are in contact.

sults and the Monte Carlo simulations for the present sample suggests that, at least for high particle volume fraction, the latter is more likely to be observed. This whole situation is illustrated in Fig. 8. Note that our results clearly suggest that, at a certain concentration range, colloids might become stable even in the presence of agglomerates. This could happen if the agglomerated nanoparticle's surfaces are as efficiently coated as the isolated nanoparticles and if the number of particles in an agglomerate is not high enough. This result should not apply only to the magnetic colloids considered in the present work, but can be generalized for several types of colloids.

The dependence of $D_{surf\text{-}surf}$ on ξ (Fig. 5) shows another interesting behavior: at higher graftings, all curves converge to the same value, while at lower graftings, they appear to be concentration dependent. The fact that $D_{surf\text{-}surf}$ does not vary consistently when the grafting is below 1×10^{17} molecules/m^2 indicates that the steric repulsion is less relevant in this limit and attractive interactions (magnetic and van der Waals) dominate. It is also interesting to note that for low grafting, the nanoparticles get closer at lower concentrations. This can be understood if we realize that the particles of a dimer can approximate more if there are not other particles in the vicinity pulling them. The closer are the other particles, the greater is the tendency of the nanoparticles of the pair to separate. A similar behavior was observed experimentally by Elói and co-workers [49]. At the high grafting limit, the steric repulsion is very high and the particles of each pair keep so separated that the attractive interaction are not relevant enough to cause this effect.

Finally it is important to discuss a little bit further the influence of the Hamaker constant. Following the Lifshitz theory [57–59], the Hamaker constant for two macroscopic bodies made of a material α interacting in a medium β can be described, in the nonretarded limit, in terms of macroscopic quantities relative to these media:

$$A \approx \frac{3}{4}k_BT\left(\frac{\varepsilon_\alpha-\varepsilon_\beta}{\varepsilon_\alpha+\varepsilon_\beta}\right)^2+\frac{3h\nu_e}{16\sqrt{2}}\frac{(\eta_\alpha^2-\eta_\beta^2)^2}{(\eta_\alpha^2+\eta_\beta^2)^{3/2}}, \qquad (13)$$

where the ε's are the electric permittivities, the η's are the indexes of refraction, h is the Planck constant, and ν_e is the main absorption frequency, considered the same for both materials. This description is possible as the electric polarizability, which determines van der Waals interactions, is also correlated with the electric permittivity ε and the index of refraction, η.

TABLE IV. Constants used to estimate the Hamaker constant following the Lifshitz theory [57–59]. ε is the electric permittivity and η the index of refraction.

Constant	Value	Reference
$\varepsilon_{Fe_3O_4}$	5.9	[60]
$\eta_{Fe_3O_4}$	2.4	[60]
$\varepsilon_{C_nH_m}$	1.3	[60]
$\eta_{C_nH_m}$	1.4	[57]
$\varepsilon_{C_{12}H_{24}O_2}$	2.7	[60]
$\eta_{C_{12}H_{24}O_2}$	1.4	[60]
ν_e (typical)	3×10^{15} Hz	[57]
ν_e (magnetite)	0.3×10^{15} Hz	[63]

In our surfacted ferrofluid system, material A is effectively composed by the magnetite cores and the dodecanoic acid surfactant. In the limit of low concentration and low grafting, the magnetite can be considered as A and the hydrocarbon as B. In the limit of high concentration and high grafting, B must be the surfactant, because it surrounds the nanoparticles instead of the hydrocarbon. Using the constants in Table IV for the calculation of A and considering $\alpha\equiv Fe_3O_4$ (magnetite) and $\beta\equiv C_nH_m$ (hydrocarbon), we obtain the correspondent Hamaker constant as $A_{magnetite\text{-}hydrocarbon}=2.05\times10^{-19}$ J using the typical value of ν_e. In a similar manner, changing the definition of B to $B\equiv C_{12}H_{24}O_2$ (dodecanoic acid), we get $A_{magnetite\text{-}dodecanoic}=2.04\times10^{-19}$ J.

Although our calculations suggest that the surfactant does not change A considerably, it is important to remember that the parameters for the dodecanoic acid are related to a liquid medium, while in our system this molecule is with the polar heads attached to the nanoparticle's surface, in a quasisolid configuration. The higher value of the index of refraction of magnetite ($\eta_{Fe_3O_4}=2.42$) when compared with other η values is mainly responsible for the higher value of the Hamaker constant obtained in this approach. It is worthy pointing out that this value is higher then the Hamaker constant usually considered by many researchers in this field [61,62] [$(0.3–2.3)\times10^{-19}$ J]. A possible reason for this difference might be the consideration of a different absorption frequency, considered the same for the two media in this model. According to Tepper and co-workers [63] the maximum absorption wavelength of magnetite is around 900 nm, which gives $\nu_e=0.3\times10^{15}$ Hz, and hence $A_{magnetite\text{-}dodecanoic}=2.07\times10^{-20}$ J and $A_{magnetite\text{-}hydrocarbon}=2.17\times10^{-20}$ J, one order of magnitude lower than the values for the typical ν_e value.

Considering this uncertainty in the theoretical prediction of A and aiming the access to the role of the Hamaker constant in the properties focused on this work, we have varied the Hamaker constant value while computing $D_{surf\text{-}surf}$ and F_{mon}. Figure 9 presents $D_{surf\text{-}surf}$ as a function of grafting for

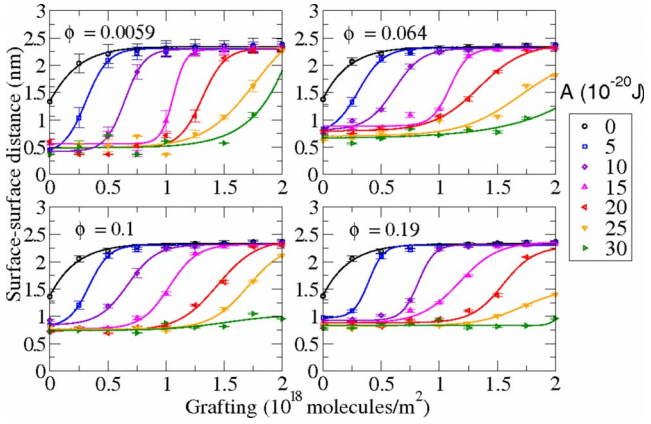

FIG. 9. (Color online) Surface-surface distance in pairs of bonded nanoparticles ($D_{surf\text{-}surf}$) versus grafting (ξ) for different Hamaker constants (A) and volume fraction (ϕ). The solid lines correspond to the adjusted function $D_{surf\text{-}surf} \propto \tanh[\alpha(\xi)]$. Black circles are for $A=0\times10^{-20}$ J, blue (dark gray) squares are for $A=5\times10^{-20}$ J, violet (middle-dark gray) diamonds are for $A=10\times10^{-20}$ J, magenta (middle-light gray) up triangles are for $A=15\times10^{-20}$ J, red (middle-dark gray) left triangles are for $A=20\times10^{-20}$ J, orange (light gray) down triangles are for $A=25\times10^{-20}$ J, and green (middle gray) right triangles are for $A=30\times10^{-20}$ J.

various Hamaker constant and concentration values. The lines represent adjusted functions $D_{surf\text{-}surf} \propto \tanh(\alpha\xi)$, as discussed for Fig. 5. It is clear that increasing the Hamaker constant value has a net effect of displacing the curves to the right. The observed fluctuations are not large, suggesting that an increase in the number of nanoparticles or changes in the convergence criteria will probably not result in substantial changes in the observed results. Basically the behavior of $D_{surf\text{-}surf}$ as a function of ξ for various graftings suggests that the mean agglomerate size increases when the Hamaker constant and the particle volume fraction increase and the grafting number decreases. The $F_{mon}\times\xi$ curves (not shown here) presented a similar behavior. The main difference, for most nanoparticle concentrations and especially the higher ones, is the fact that the experimental values of F_{mon} were not reached by the curves adjusted to the simulation points corresponding to $A>0.5\times10^{-19}$ J in the analyzed physically meaning grafting range of $(0-2)\times10^{18}$ molecules/m^2. This reinforces the reasonability of the initially chosen Hamaker constant $A=0.4\times10^{-19}$ J. Those parameters are certainly of crucial importance in many types of colloids with similar particle sizes.

Finally it would be interesting to comment that many theoretical models from the literature, usually, only take into account the dipolar interaction term to the formation of nanoparticle chains [23,56,64,65]. Nevertheless, our results, as well as a previous one by Kruse *et al.* [15], clearly show that van der Waals and steric interaction terms play a key role on chain formation. Therefore we conclude that better agreement between experiment and theory might be achieved through the inclusion of these terms, which are also extremely important on the stability of several types of colloids.

IV. SUMMARY

In this work, we investigated samples of a polydisperse magnetic fluid, composed of Fe_3O_4-based nanoparticles surface coated with dodecanoic acid molecules and dispersed in a hydrocarbon solvent. Through a comparison of three-dimensional Monte Carlo simulations and EMR measurements, it was possible to investigate the behavior of the surfactant dodecanoic acid molecules. Based on a modified Langmuir model, the role of surfactant molecules is investigated. The dependence of the grafting of monomers and agglomerated nanoparticles with concentration was obtained, suggesting that the grafting (surface density of surfactant molecules) of isolated particles tends to increase with increasing particle concentration, while the grafting of bonded nanoparticles shows a more complicated behavior probably due to entanglement effects. From our analysis it was possible to suggest that when a pair of nanoparticles get close enough to put their surfactant layers in contact, the adsorbed molecules are taken out of their previous stability and tend to dissociate from the surfaces of the nanoparticles. As the polar heads of the dissociated molecules are repelled by the apolar solvent, these molecules are more likely to adsorb on available adsorption sites. The effects of the steric repulsion and the van der Waals attraction were also explored by varying the grafting and the Hamaker constant over a wide range. For low grafting, the surface-surface distance between bonded nanoparticles tends to increase with increasing concentration, in agreement with previous experimental observations, revealing that the influence of the nanoparticles in the vicinity of a dimer tends to separate them. Indeed, both parameters, the Hamaker constant and the grafting number, play a key role in the formation of agglomerates and the stability of the colloid.

ACKNOWLEDGMENTS

The authors acknowledge financial support from CAPES, CNPq, DPP-UnB, IF-UFG, and FUNAPE.

[1] P. Hermetin, R. Doenges, U. Franssen, C. Bieva, F. J. Vander Brugghen, P. Stryckmans, H. J. Friesen, B. Optaczy, and S. Schneider, Bioconjugate Chem. **1**, 411 (1990).

[2] A. Kuznetsov, V. I. Filippov, O. A. Kuznetsov, V. G. Gerlivanov, E. K. Dobrinsky, and S. I. Malashin, J. Magn. Magn. Mater. **194**, 22 (1999).

[3] J. Yang, C.-H. Lee, J. Park, S. Seo, E.-K. Lim, Y. J. Song, J.-S. Suh, H.-G. Yoon, Y.-M. Huh, and S. Haam, J. Mater. Chem. **17**, 2695 (2007).

[4] M. Bonini, A. Wiedenmannb, and P. Baglioni, J. Appl. Crystallogr. **40**, S254 (2007).

[5] P. C. Morais, S. W. da Silva, M. A. G. Soler, and N. Buske, J.

Phys. Chem. **104**, 2894 (2000).
[6] P. C. Morais, S. W. da Silva, M. A. G. Soler, and N. Buske, Biomol. Eng. **17**, 41 (2001).
[7] S. W. da Silva, M. A. G. Soler, G. Gansau, N. Buske, and P. C. Morais, J. Magn. Magn. Mater. **226-230**, 1890 (2001).
[8] B. Huke and M. Lücke, Rep. Prog. Phys. **67**, 1731 (2004).
[9] R. W. Chantrell, A. Bradbury, J. Popplewell, and S. W. Charles, J. Appl. Phys. **53**, 2742 (1982).
[10] P. J. Camp and G. N. Patey, Phys. Rev. E **62**, 5403 (2000).
[11] R. W. Chantrell, G. N. Coverdale, M. El Hilo, and K. O'Grady, J. Magn. Magn. Mater. **157-158**, 250 (1996).
[12] A. Satoh, R. W. Chantrell, S.-I. Kamiyama, and G. N. Coverdale, J. Colloid Interface Sci. **181**, 422 (1996).
[13] J. O. Andersson, C. Djurberg, T. Jonsson, P. Svedlindh, and P. Nordblad, Phys. Rev. B **56**, 13983 (1997).
[14] A. Satoh and S.-I. Kamiyama, J. Colloid Interface Sci. **172**, 37 (1995).
[15] T. Kruse, A. Spanoudaki, and R. Pelster, Phys. Rev. B **68**, 054208 (2003).
[16] T. Kristof and I. Szalai, Phys. Rev. E **68**, 041109 (2003).
[17] P. Vargas, D. Altbir, J. d'Albuquerque e Castro, Phys. Rev. B **73**, 092417 (2006).
[18] D. Kechrakos and K. N. Trohidou, Phys. Rev. B **74**, 144403 (2006).
[19] H. F. Du and A. Du, Phys. Status Solidi B **244**, 1401 (2007).
[20] H. K. Lee, T. C. Schulthess, D. P. Landau, G. Brown, J. P. Pierce, Z. Gai, G. A. Farnan, and J. Shen, J. Appl. Phys. **91**, 6926 (2002).
[21] T. Kruse, H. G. Krauthauser, A. Spanoudaki, and R. Pelster, Phys. Rev. B **67**, 094206 (2003).
[22] A. Ghazali and J.-C. Levy, Phys. Rev. B **67**, 064409 (2003).
[23] P. De Gennes and P. Pincus, Phys. Kondens. Mater. **11**, 189 (1970).
[24] P. C. Scholten, IEEE Trans. Magn. **16**, 221 (1980).
[25] A. F. Bakuzis, M. F. da Silva, P. C. Morais, L. S. F. Olavo, and K. Skeff Neto, J. Appl. Phys. **87**, 2497 (2000).
[26] A. F. Pshenichnikov and A. A. Fedorenko, J. Magn. Magn. Mater. **292**, 332 (2005).
[27] S. Kantorovich and A. O. Ivanov, J. Magn. Magn. Mater. **252**, 244 (2002).
[28] A. O. Ivanov and S. S. Kantorovich, Colloid J. **65**, 166 (2003).
[29] A. O. Ivanov, Z. Wang, and C. Holm, Phys. Rev. E **69**, 031206 (2004).
[30] E. L. Mackor, J. Colloid Sci. **6**, 492 (1951).
[31] R. E. Rosensweig, *Ferrohydrodynamics* (Dover, New York, 1997).
[32] M. S. Seehra, H. Shim, P. Dutta, A. Manivannan, and J. Bonevich, J. Appl. Phys. **97**, 10J509 (2005).
[33] R. J. Usselman, M. T. Klem, M. Allen, E. D. Walter, K. Gilmore, T. Douglas, M. Young, Y. Idzerda, and D. J. Singel, J. Appl. Phys. **97**, 10M523 (2005).
[34] R. Berger, J. Kliava, J. C. Bissey, and V. Baietto, J. Appl. Phys. **87**, 7389 (2000).
[35] A. R. Pereira, K. L. C. Miranda, P. P. C. Sartoratto, P. C. Morais, and A. F. Bakuzis, J. Appl. Phys. **100**, 086110 (2006).
[36] P. C. Morais, M. C. F. L. Lara, A. L. Tronconi, F. A. Tourinho, A. R. Pereira, and F. Pelegrini, J. Appl. Phys. **79**, 7931 (1996).
[37] A. F. Bakuzis, P. C. Morais, and F. Pelegrini, J. Appl. Phys. **85**, 7480 (1999).
[38] A. F. Bakuzis, A. R. Pereira, J. G. Santos, and P. C. Morais, J. Appl. Phys. **99**, 08C301 (2006).
[39] G. R. R. Gonçalves, A. F. Bakuzis, K. Skeff Neto, F. Pelegrini, and P. C. Morais, J. Magn. Magn. Mater. **289**, 142 (2005).
[40] D. Gunter and N. Buske, DE Patent No. 4325386 (1993).
[41] N. Metropolis, A. Rosenbluth, M. Rosenbluth, A. Teller, and E. Teller, J. Chem. Phys. **21**, 1087 (1953).
[42] H. C. Hamaker, Physica (Amsterdam) **4**, 1058 (1937).
[43] K. Skeff Neto, A. F. Bakuzis, G. R. R. Gonçalves, F. Pelegrini, and P. C. Morais, J. Magn. Magn. Mater. **289**, 129 (2005).
[44] L. L. Castro, M. F. da Silva, A. F. Bakuzis, and R. Miotto, J. Magn. Magn. Mater. **293**, 553 (2005).
[45] M. Porto, J. Appl. Phys. **92**, 6057 (2002).
[46] A. O. Ivanov, S. S. Kantorovich, E. N. Reznikov, C. Holm, A. F. Pshenichnikov, A. V. Lebedev, A. Chremos, and P. J. Camp, Phys. Rev. E **75**, 061405 (2007).
[47] K. Chen, A. F. Bakuzis, and W. Luo, Appl. Surf. Sci. **252**, 6379 (2006).
[48] M. Klokkenburg, J. Hilhorst, and B. H. Ern, Vib. Spectrosc. **43**, 243 (2007).
[49] M. T. A. Elói, R. B. Azevedo, E. C. D. Lima, A. C. M. Pimenta, and P. C. Morais, J. Magn. Magn. Mater. **293**, 220 (2005).
[50] A. F. Bakuzis, K. Skeff Neto, P. P. Gravina, L. C. Figueiredo, P. C. Morais, L. P. Silva, R. B. Azevedo, and O. Silva, Appl. Phys. Lett. **84**, 2355 (2004).
[51] S. Taketomi, M. Ukita, M. Mizukami, H. Miyajima, and S. Chikazumi, J. Phys. Soc. Jpn. **56**, 3362 (1987).
[52] G. D. Benicio, F. Pelegrini, A. F. Bakuzis, K. L. C. Miranda, and P. P. C. Sartoratto, J. Appl. Phys. **101**, 09J106 (2007).
[53] When the magnetic resonance field is plotted as a function of the particle volume fraction data (see, for example, Fig. 2 in Ref. [39]), a clear decreasing of $D_{surf\text{-}surf}$ is observed.
[54] A. Zangwill, *Physics at Surfaces* (Cambridge University Press, Cambridge, England, 1992).
[55] R. J. Hunter, *Introduction to Modern Colloid Science* (Oxford University Press, New York, 1994).
[56] A. Y. Zubarev and L. Y. Iskakova, Phys. Rev. E **61**, 5415 (2000).
[57] J. Israelachvili, *Intermolecular and Surface Forces* (Academic Press, London, 1992).
[58] E. M. Lifshitz, Sov. Phys. JETP **2**, 73 (1956).
[59] I. E. Dzyaloshinskii, E. M. Lifshitz, and L. P. Pitaevskii, Adv. Phys. **10**, 165 (1961).
[60] *Handbook of Chemistry and Physics*, 87th ed., edited by D. R. Lide *et al.* (CRC Press, Boca Raton, 2007).
[61] B. M. Berkovsky, V. F. Medvedev, and M. S. Krakov, *Magnetic Fluids: Engineering Applications* (Oxford University Press, New York, 1993).
[62] R. Tadmor, R. E. Rosensweig, J. Frey, and J. Klein, Langmuir **16**, 9117 (2000).
[63] T. Tepper, C. A. Ross, and G. F. Dionne, IEEE Trans. Magn. **40**, 1685 (2004).
[64] P. C. Jordan, Mol. Phys. **25**, 961 (1973).
[65] V. S. Mendelev and A. O. Ivanov, Phys. Rev. E **70**, 051502 (2004).